

Tailoring-compensated ferrimagnetic state and anomalous Hall effect in quaternary Mn-Ru-V-Ga Heusler compounds

Jin-Jing Liang(梁瑾静), Xue-Kui Xi(郗学奎), Wen-Hong Wang(王文洪), and Yong-Chang Lau(刘永昌)

Citation: Chin. Phys. B, 2024, 33 (**7**): 077504. DOI: 10.1088/1674-1056/ad34c8
Journal homepage: http://cpb.iphy.ac.cn; http://iopscience.iop.org/cpb

What follows is a list of articles you may be interested in

Enhanced anomalous Hall effect in kagome magnet $YbMn_6Sn_6$ with intermediate-valence ytterbium

Longfei Li(李龙飞), Shengwei Chi(迟晟玮), Wenlong Ma(马文龙), Kaizhen Guo(郭凯臻), Gang Xu(徐刚), and Shuang Jia(贾爽)
Chin. Phys. B, 2024, 33 (**5**): 057501. DOI: 10.1088/1674-1056/ad322d

Angular and planar transport properties of antiferromagnetic V_5S_8

Xiao-Kai Wu(吴晓凯), Bin Wang(王彬), De-Tong Wu(吴德桐), Bo-Wen Chen(陈博文), Meng-Juan Mi(弭孟娟), Yi-Lin Wang(王以林), and Bing Shen(沈冰)
Chin. Phys. B, 2024, 33 (**2**): 027503. DOI: 10.1088/1674-1056/ad15f9

Magnetic and electronic properties of bulk and two-dimensional $FeBi_2Te_4$: A first-principles study

Qianqian Wang(王倩倩), Jianzhou Zhao(赵建洲), Weikang Wu(吴维康), Yinning Zhou(周胤宁), Qile Li, Mark T. Edmonds, and Shengyuan A. Yang(杨声远)
Chin. Phys. B, 2023, 32 (**8**): 087506. DOI: 10.1088/1674-1056/acd522

Topological magnetotransport and electrical switching of sputtered antiferromagnetic $Ir_{20}Mn_{80}$

Danrong Xiong(熊丹荣), Yuhao Jiang(蒋宇昊), Daoqian Zhu(朱道乾), Ao Du(杜奥), Zongxia Guo(郭宗夏), Shiyang Lu(卢世阳), Chunxu Wang(王春旭), Qingtao Xia(夏清涛), Dapeng Zhu(朱大鹏), and Weisheng Zhao(赵巍胜)
Chin. Phys. B, 2023, 32 (**5**): 057501. DOI: 10.1088/1674-1056/acb9ec

Optimized growth of compensated ferrimagnetic insulator $Gd_3Fe_5O_{12}$ with a perpendicular magnetic anisotropy

Heng-An Zhou(周恒安), Li Cai(蔡立), Teng Xu(许腾), Yonggang Zhao(赵永刚), and Wanjun Jiang(江万军)
Chin. Phys. B, 2021, 30 (**9**): 097503. DOI: 10.1088/1674-1056/ac0db0

Tailoring-compensated ferrimagnetic state and anomalous Hall effect in quaternary Mn–Ru–V–Ga Heusler compounds

Jin-Jing Liang(梁瑾静)[1,2], Xue-Kui Xi(郗学奎)[1], Wen-Hong Wang(王文洪)[3], and Yong-Chang Lau(刘永昌)[1,2,†]

[1] *Beijing National Laboratory for Condensed Matter Physics, Institute of Physics, Chinese Academy of Sciences, Beijing* 100190, *China*
[2] *University of Chinese Academy of Sciences, Beijing* 100049, *China*
[3] *Tiangong University, Tianjin* 300387, *China*

(Received 22 January 2024; revised manuscript received 7 March 2024; accepted manuscript online 18 March 2024)

Cubic Mn_2Ru_xGa Heusler compound is a typical example of compensated ferrimagnet with attractive potential for high-density, ultrafast, and low-power spintronic applications. In the form of epitaxial thin films, Mn_2Ru_xGa exhibits high spin polarization and high tunability of compensation temperature by freely changing the Ru content x in a broad range ($0.3 < x < 1.0$). Herein Mn–Ru–Ga-based polycrystalline bulk buttons prepared by arc melting are systematically studied and it is found that in equilibrium bulk form, the cubic structure is unstable when $x < 0.75$. To overcome this limitation, Mn–Ru–Ga is alloyed with a fourth element V. By adjusting the content of V in the $Mn_2Ru_{0.75}V_yGa$ and $Mn_{2.25-y}Ru_{0.75}V_yGa$ quaternary systems, the magnetic compensation temperature is tuned. Compensation is achieved near 300 K which is confirmed by both the magnetic measurement and anomalous Hall effect measurement. The analyses of the anomalous Hall effect scaling in quaternary Mn–Ru–V–Ga alloy reveal the dominant role of skew scattering, notably that contributed caused by the thermally excited phonons, in contrast to the dominant intrinsic mechanism found in many other 3d ferromagnets and Heusler compounds. It is further shown that the Ga antisites and V content can simultaneously control the residual resistivity ratio (RRR) as well as the relative contribution of phonon and defect to the anomalous Hall effect a''/a' in Mn–Ru–V–Ga, resulting in a scaling relation $a''/a' \propto \mathrm{RRR}^{1.8}$.

Keywords: compensated ferrimagnet, anomalous Hall effect, residual resistivity ratio

PACS: 75.20.En, 75.50.Gg, 75.47.–m **DOI:** 10.1088/1674-1056/ad34c8

1. Introduction

Ferrimagnets, which consist of inequivalent antiferromagnetically coupled magnetic sublattices, have become one of the most attractive material classes in spintronics[1–7] because they combine the advantages of ferromagnets and antiferromagnets. On one hand, the ferromagnet-like electrical properties of ferrimagnets can be more easily used to achieve electrical reading and writing, compared to antiferromagnets.[3] On the other hand, ferrimagnets show antiferromagnet-like dynamics and they may switch much faster than ferromagnets.[7] Moreover, inequivalent magnetic sublattices exhibit different temperature dependence, so that in some cases, a full magnetic compensation may appear in a so-called compensated ferrimagnet. The temperature at which the net magnetization vanishes is the magnetic compensation temperature (T_M). Compensated ferrimagnets which show no stray fields, high spin polarization, large anomalous Hall effect, and low damping at room temperature have attractive potential applications in high-density, ultrafast, and low-power spintronics.[8–16]

The common ferrimagnets include rare-earth iron garnets,[17–19] rare-earth transition metal alloys,[20–22] Mn_4N-based nitrides,[23,24] and some Mn-based Heusler compounds.[25–31] By varying the composition, not only can the compensated ferrimagnetic state be achieved, but also T_M can be regulated. Cubic Mn_2Ru_xGa thin film is a typical example of compensated ferrimagnet with high spin polarization and high tunability of T_M by freely varying the Ru content x in a broad range ($0.3 < x < 1.0$).[27] So far, Mn–Ru–Ga alloy has mostly been realized in the form of thin films, such as epitaxial growth on MgO substrates,[27,30,32] which is known to be a popular method of stabilizing metastable phases of matter. It remains unclear to what extent is the cubic Mn–Ru–Ga ternary alloy thermodynamically stable and how the atomic order evolves as a function of x. Another important feature of the compensated ferrimagnet is the emergence of finite anomalous Hall effect, even when the net magnetization exactly vanishes. The existing compensated ferrimagnetic thin films, however, typically show mediocre change of the longitudinal resistance with temperature[27,33] and complex anomalous Hall effect loops[34–37] which impede accurate extraction of the anomalous Hall effect scaling. The aforementioned issues motivate us to study the Mn–Ru–Ga-based ternary alloys and Mn–Ru–V–Ga quaternary alloys in bulk form.

We find that the cubic Heusler structure of Ru-deficient Mn_2Ru_xGa and $Mn_{3-x}Ru_xGa$ bulk alloys becomes unstable for $x < 0.75$. Alloying with vanadium stabilizes the cubic structure of Mn–Ru–V–Ga and enables tunable compensated ferrimagnetic state in a wider temperature range, including

†Corresponding author. E-mail: yongchang.lau@iphy.ac.cn
© 2024 Chinese Physical Society and IOP Publishing Ltd

room temperature. Moreover, although they are a ternary or quaternary alloy system, our polycrystalline bulk samples exhibit appreciable residual resistivity ratio (RRR) ranging from 2 to 5 (compared to previous thin film samples), allowing us to comfortably study the scaling relation of the anomalous Hall effect. We find nonnegligible thermally activated phonon contribution to the extrinsic anomalous Hall effect in these compensated ferrimagnets and establish a link between the RRR and the relative contribution of phonon and defect to the anomalous Hall effect.

2. Experimental techniques

Polycrystalline buttons of Mn_2Ru_xGa, $Mn_{3-x}Ru_xGa$, $Mn_2Ru_{0.75}V_yGa$, and $Mn_{2.25-y}Ru_{0.75}V_yGa$ were prepared by arc melting. Extra 5% of Mn has been added to compensate for the losses. Samples were repeatedly melted four times after flipping to ensure the homogeneity. $Mn_2Ru_{0.75}V_yGa$ and $Mn_{2.25-y}Ru_{0.75}V_yGa$ ($0 \leq y \leq 0.25$) samples were sealed inside quartz tubes evacuated to 2×10^{-4} Pa, annealed at 1073 K for 7 days, and then cooled to room temperature for one day to improve the atomic ordering. The crystal structure was determined by the powder x-ray diffraction (XRD). The density was measured by the Archimedes drainage method. Magnetic properties were measured by using the Quantum Design magnetic property measurement system in SQUID-VSM mode. Magnetotransport properties were measured by using standard 6 contact method on thin slab samples with a typical thickness of $\sim$ 100 μm in a physical property measurement system.

3. Results and discussion

3.1. Magnetic compensation in ferrimagnetic Mn–Ru–Ga alloys

Figure 1(a) illustrates the crystal structure of the stoichiometric and atomically-ordered Mn_2RuGa. Ru occupies 4*d* sites, Ga is on 4*b* sites and Mn occupies inequivalent 4*c* and 4*a* sites, thus forming the noncentrosymmetric Hg_2CuTi-type inverse Heusler structure (Space group No. 216).[38] For quaternary Mn–Ru–V–Ga alloy, small amount of V with stronger affinity to Ga is expected to preferably replace some of the Mn atoms on 4*a* sites. The magnetism of the compound is mainly governed by the antiferromagnetically coupled 4*a* and 4*c* Mn sublattices that are inequivalent in terms of chemical environment and atomic occupancy.[29] The basic concept of the magnetization compensation in a compensated ferrimagnet that consists of antiferromagnetically coupled M_1 and M_2 magnetic sublattices is depicted in Fig. 1(b). The inequivalent M_1 and M_2 sublattices exhibit different total moment M at 0 K and dissimilar temperature dependency. As the temperature increases, if the sublattice with smaller M at 0 K (here M_1) shows weaker temperature dependence than M_2 sublattice, magnetic compensation may occur at the crossover T_M where the magnetizations of M_1 and M_2 sublattices are equal in magnitude but opposite in sign. Below T_M, the net moment of the compound is governed by the M_2 sublattice, whereas above T_M, M_1 sublattice is dominant. In order to adapt a given application, it is desirable to be able to regulate the T_M over large temperature range. In the following subsections, such an ability will be demonstrated for quaternary Mn–Ru–V–Ga compound.

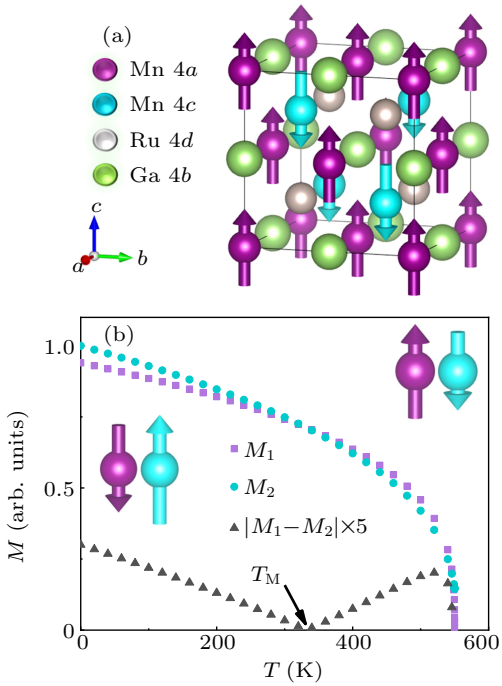


Fig. 1. Crystal structure of cubic Mn_2RuGa, showing that moments of Mn at 4*a* and 4*c* sites are aligned in antiparallel manner. (b) Concept of magnetic compensation at compensation temperature T_M for a compensated ferrimagnet, showing temperature dependence of magnetization of the two sublattices M_1 and M_2 and the net magnetization $|M_1 - M_2|$. The latter is magnified 5 times for clarity.

3.2. Structural characterizations

We first study ternary Mn–Ru–Ga-based polycrystalline buttons Mn_2Ru_xGa and $Mn_{3-x}Ru_xGa$ in the form of equilibrium bulk. The nominal compositions of the former series are similar to that studied by Kurt *et al.*[27] in the form of epitaxial thin films. This series is considered off-stoichiometric because the Ga concentration is higher than the ideal 25 at.% for a full Heusler compound of general formula X_2YZ (Z being a main group element). For comparison, we also prepare the latter sample series with nominal Ga concentration fixed at 25 at.%. In Figs. 2(a) and 2(b), we show the powder XRD of as-cast Mn_2Ru_xGa and $Mn_{3-x}Ru_xGa$. When x is less than 0.75, these alloys are no longer in a pure cubic phase. Peaks that correspond to the tetragonal and hexagonal phases appear in $Mn_2Ru_{0.5}Ga$, and the parasitic tetragonal phase emerges in $Mn_{2.5}Ru_{0.5}Ga$. Furthermore, we did not succeed in suppressing these parasitic phases by post annealing. We therefore

conclude that the cubic structure is unstable for the two series when $x < 0.75$, which substantially reduces the tunability of bulk Mn–Ru–Ga ferrimagnet, notably T_M cannot be tuned to room temperature.

Referring to the Slater–Pauling rule,[39–41] the magnetic moment M at 0 K of an X_2YZ half-metal with $L2_1$ full Heusler structure follows $M = N_v - 24$ (N_v is the number of valence electrons per formula). Alloying a fourth element (e.g., Ti, V, Cr) with less valence electrons than Mn and Ru into Mn_2Ru_xGa ($M = 1\ \mu_B$/f.u. for $x = 1$) may extend the tuning range of T_M. We choose and alloy Mn–Ru–Ga with V because Mn_2VGa was known to be a cubic Heusler with a high Curie temperature of 783 K.[43] In contrast, since Mn_2CrGa does not crystallize into cubic structure,[42] and there is, to the best of our knowledge, no experimental report on Mn_2TiGa, alloying with Cr and Ti may not be as favorable as V in terms of phase stability. By fixing the Ru concentration at $x = 0.75$, we systematically investigate $Mn_2Ru_{0.75}V_yGa$ and $Mn_{2.25-y}Ru_{0.75}V_yGa$ quaternary systems. Again, the former series is off-stoichiometric in terms of Ga, whereas the latter series nominally fixes 25 at.% of Ga.

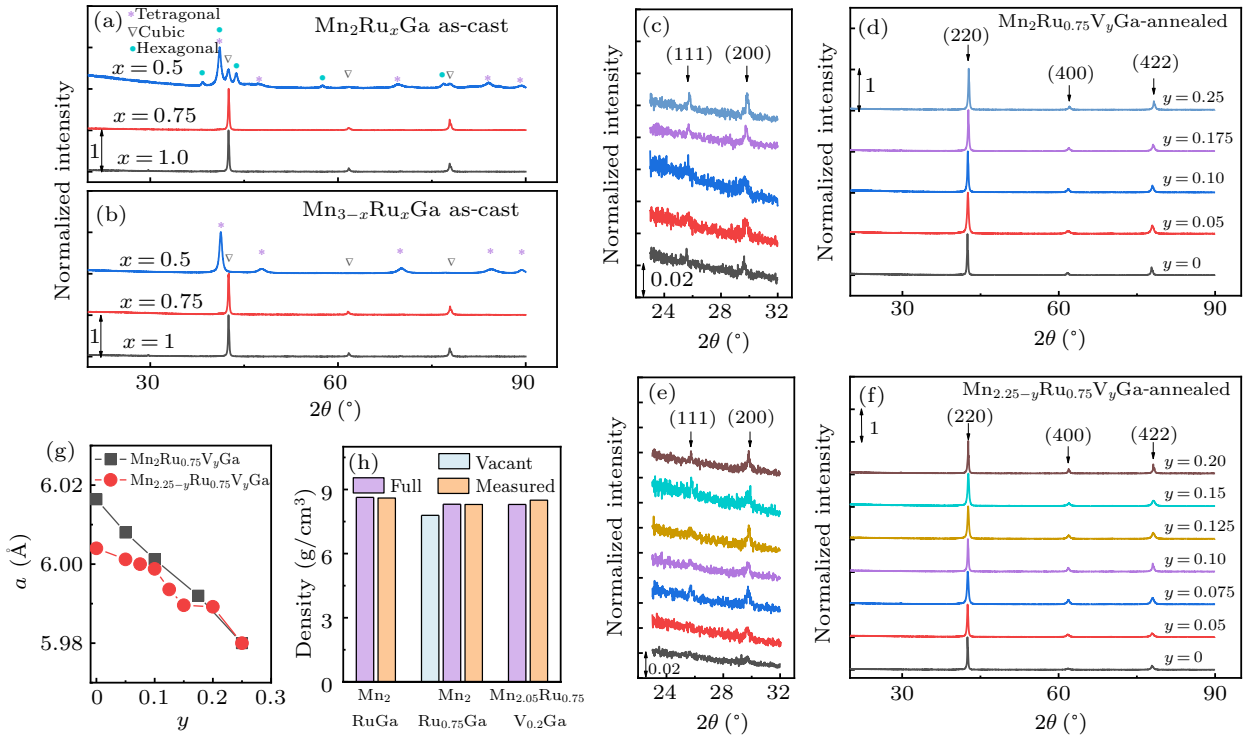


Fig. 2. Powder XRD patterns for (a) as-cast Mn_2Ru_xGa, (b) as-cast $Mn_{3-x}Ru_xGa$, (d) annealed $Mn_2Ru_{0.75}V_yGa$, and (f) annealed $Mn_{2.25-y}Ru_{0.75}V_yGa$. Zoom-in views at low 2θ angles are shown for (c) annealed $Mn_2Ru_{0.75}V_yGa$ and (e) annealed $Mn_{2.25-y}Ru_{0.75}V_yGa$. (g) Lattice parameter a against V concentration y. (h) Comparison of measured density with density calculated from structural models with fully atomic occupancy (full) and with vacancy (vacant).

The powder XRD spectra for the two series after annealing are plotted in Figs. 2(d) and 2(f). All the samples crystallize in the cubic phase without showing noticeable parasitic phase. We observe strong reflections that can be indexed by the (hkl) Bragg peaks satisfying the relation $h + k + l = 4n$ (n = integer). As shown in Fig. 2(g), the steady and monotonically decreasing trend of the extracted lattice parameter a with the increase of V composition y provides another evidence of systematic alloying. In addition, as shown in the enlarged XRD patterns for 2θ ranging from 23° to 32° [Figs. 2(c) and 2(e)], weak superlattice peaks corresponding to the (111) and (200) reflections are clearly visible. This mainly indicates that the position of the heaviest Ru atoms is at least partially ordered. Note that we do not intend to estimate the ordering parameter of these samples because additional assumptions must be made, that is, how other atoms are ordered and whether an atomic site is always fully occupied, with a total atomic occupancy always being equal to 1.

In fact, the actual atomic ordering and occupancy of Mn_2Ru_xGa are still controversial. In the pioneering work by Kurt *et al.*,[27] Mn_2Ru_xGa was assumed to be an intermediate compound between the half Heusler and inverse Heusler structure, where Ru gradually fills the empty 4d site until $x = 1$. More recently, according to the thin film density estimated from the critical angle of the x-ray reflectivity data, Siewierska *et al.*[28] showed that all the investigated Mn–Ru–Ga films adopt full atomic occupancy with no obvious sign of vacancy. Herein, these Heusler compounds are successfully synthesized in the form of bulk buttons, enabling us to independently and directly measure the density of these samples by using the Archemede drainage method. For the three selected samples, their measured density is compared with the

expected density in the cases of full atomic occupancy (full) and with atomic vacancy (vacant), as shown in Fig. 2(h). Experimental data support the scenario with full atomic occupancy in all cases, with and without V alloying. Next, we shall focus on the magnetic and magnetotransport characterizations of $Mn_2Ru_{0.75}V_yGa$ and $Mn_{2.25-y}Ru_{0.75}V_yGa$ quaternary compounds for $0 \leq y \leq 0.25$.

3.3. Magnetic properties

The magnetic properties of the off-stoichiometric $Mn_2Ru_{0.75}V_yGa$ for $0 \leq y \leq 0.25$ are summarized in Fig. 3. The magnetization M measured on cooling with an applied magnetic field of 0.1 T is plotted against temperature T in Fig. 3(a). For all the samples, M values remain finite at 400 K, indicating that the Curie temperatures of these compounds is well above 400 K. As the temperature decreases, M first decreases to about zero and then increases. This is an indication of the magnetic compensation as explained in Fig. 1(b). To further confirm the compensation characteristics, we first apply a magnetic field of 0.5 T above the compensation temperature to magnetize the sample, and then remove the magnetic field to measure the temperature dependence of magnetization $M(T)$ at zero magnetic field (i.e., in remanence) on cooling. These zero-field-cooled remanent $M(T)$ curves are shown in the inset of Fig. 3(b), which directly confirm the magnetic compensation feature with the abscissa of the zero-moment point being the T_M. The T_M of all the measured samples is summarized in Fig. 3(b). Adding V consistently reduces T_M from 380 K to 260 K. For $y = 0.1$ and $y = 0.175$, the T_M is close to room temperature.

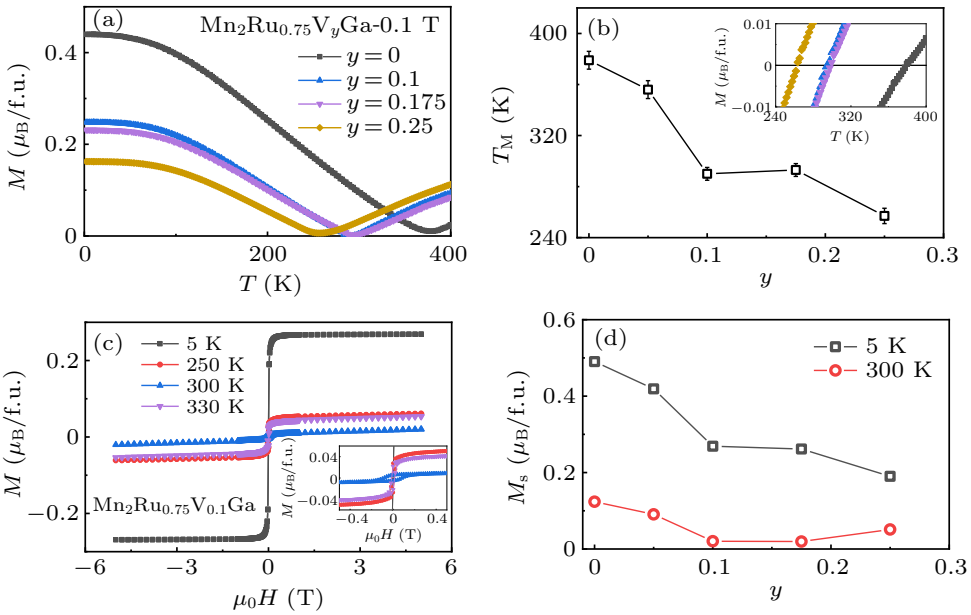


Fig. 3. (a) Temperature dependence of magnetization $M(T)$ for selected $Mn_2Ru_{0.75}V_yGa$ samples measured with a magnetic field of 0.1 T. (b) Compensation temperature T_M as a function of V content y, with inset showing $M(T)$ curves measured during cooling after removing the magnetic field. (c) $M(H)$ hysteresis loops of $Mn_2Ru_{0.75}V_{0.1}Ga$ at different temperatures, with inset showing enlarged M–H loops at low fields. (d) Variations of saturation magnetization M_s with y at 5 K and 300 K.

The magnetic field dependence of magnetization $M(H)$ for $Mn_2Ru_{0.75}V_{0.1}Ga$ (i.e., $y = 0.1$) measured at different temperatures are shown in Fig. 3(c). The inset shows the enlarged M–H loops in the low field region. The M–H loop at 300 K only shows a modest increase of the coercivity (< 0.1 T) due to the vanishing net magnetization. This is in contrast to the previous reports where biaxially-strained thin film samples grown on MgO (001) substrates tend to show huge or even diverging coercivity (> 9 T) near T_M.[28] We infer that our annealed bulk samples are mostly relaxed with negligible tetragonal distortion and the weak magnetocrystalline anisotropy is solely provided by the cubic structure. Figure 3(d) summarizes the variations of magnetization at saturation M_s with y at 5 K and 300 K. As y increases, M_s at 5 K decreases monotonically, whereas M_s at 300 K first decreases and then increases due to the crossing of T_M.

The magnetic properties of the stoichiometric $Mn_{2.25-y}Ru_{0.75}V_yGa$ series are shown in Fig. 4. Similar to Fig. 3, T_M for this sample series can be obtained from the $M(T)$ curves measured with an applied magnetic field of 0.1 T as shown in Fig. 4(a) or from the remanent $M(T)$ curves measured under zero-field-cooled condition as plotted in the inset of Fig. 4(b). The extracted T_M against V composition y is shown in Fig. 4(b). Again, T_M tends to decrease with the increase of V content y. For $y = 0$ (i.e., $Mn_{2.25}Ru_{0.75}Ga$), the higher Mn content than $Mn_2Ru_{0.75}Ga$ further enhances T_M to above 400 K. To counterbalance this trend, a higher amount of V content ($y = 0.2$) is needed to achieve compensation near 300 K for this series.

Figure 4(c) shows the magnetic field dependence of mag-

netization $M(H)$ of $Mn_{2.05}Ru_{0.75}V_{0.2}Ga$ at different temperatures. The inset shows the enlarged M–H loops at low fields, again reflecting a weak enhancement of coercivity near T_M. Figure 4(d) summarizes the variation of M_s with y at 5 K and 300 K. Similar to the T_M, as y increases, M_s at 5 K and 300 K first decreases, then it slightly increases (for $y \sim 0.15$), and finally it decreases again. The nonmonotonic change in the magnetic property with the increase of y (but not shown in the lattice constant [see Fig. 1(g)]) may be attributed to the preferred site occupancy of V that varies as y evolves, which in turn adjusts the site-specific occupancy of the two inequivalent, antiferromagnetically couple Mn sites. The magnetic compensation conditions are known to be very sensitive to such a change. Additional element-specific measurements, such as the anomalous XRD and the x-ray magnetic circular dichroism or the site-specific characterization such as the nuclear magnetic resonance are however required to verify this hypothesis.

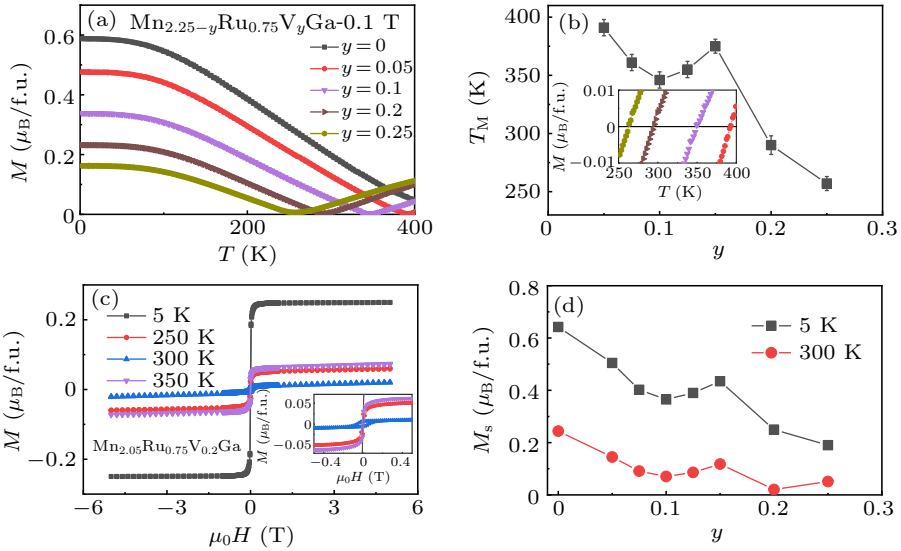


Fig. 4. (a) Temperature dependence of magnetization $M(T)$ for selected $Mn_{2.25-y}Ru_{0.75}V_yGa$ samples with a magnetic field of 0.1 T for various y values. (b) Variation of compensation temperature T_M with V content y, with inset showing the $M(T)$ curves measured during cooling after removing magnetic field. (c) The magnetic field dependence of magnetization $M(H)$ for $Mn_{2.05}Ru_{0.75}V_{0.2}Ga$ at different temperatures, with inset showing enlarged M–H loops at low fields. (d) Variation of saturation magnetization M_s with y at 5 K and 300 K.

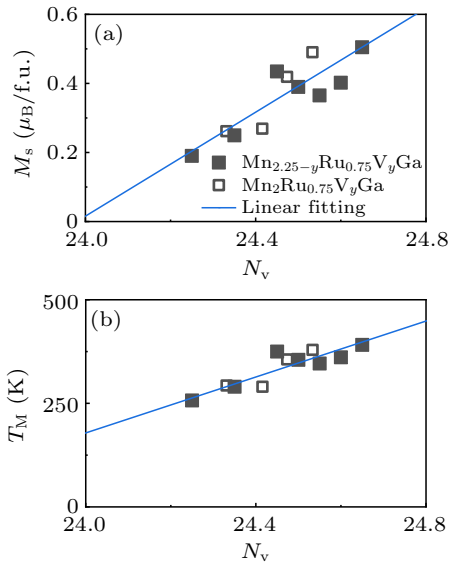


Fig. 5. Evolution of (a) saturation magnetization M_s at 5 K and (b) compensation temperature T_M with total number of valence electrons N_v. Solid and open symbols represent stoichiometric $Mn_{2.25-y}Ru_{0.75}V_yGa$ and off-stoichiometric $Mn_2Ru_{0.75}V_yGa$ series, respectively. Blue lines denote linear fits to all the data points.

Figure 5(a) summarizes the evolution of M_s at 5 K with the total number of valence electrons, N_v for the two sample series. The solid symbol and open symbol represent data points obtained from the stoichiometric $Mn_{2.25-y}Ru_{0.75}V_yGa$ and off-stoichiometric $Mn_2Ru_{0.75}V_yGa$, respectively. Note that N_v is calculated based on the structural model with full atomic occupancy without vacancy as deduced from the density measurement. We find that N_v for all samples is greater than 24 and the data from the two sample sets can be combined and described by a linear fit. By extrapolating the linear fitting line, M_s is close to zero when N_v approaches 24, which is consistent with Slater–Pauling curve. However, the slope of the linear fitting line is 0.76 ± 0.12 μ_B/f.u./electron (less than 1), suggesting that these quaternary alloys are not half-metals. Figure 5(b) summarizes the variation of T_M with N_v. Overall, as N_v decreases, T_M decreases from above 400 K to 260 K for $Mn_2Ru_{0.75}V_{0.25}Ga$. The compensation at room temperature is realized by adjusting the V content and changing N_v to about 24.4. Furthermore, the data from the two sample series with different Ga atomic ratios are naturally reconciled when N_v deduced from the fully occupied structural model is considered.

3.4. Magnetotransport properties

The Hall loops of the $Mn_2Ru_{0.75}V_{0.1}Ga$ and the $Mn_{2.05}Ru_{0.75}V_{0.2}Ga$ thin slabs measured at different temperatures are shown in Figs. 6(a) and 6(b). The ρ_{yx} is the Hall

resistivity measured with an applied magnetic field perpendicular to the slab plane. The sign reversal of the anomalous Hall effect provides another evidence that the magnetic compensation is indeed achieved near 300 K. The normal Hall coefficient strongly depends on the temperature, indicating that the Fermi level lies close to the band edge. Similar results are reported for Mn–Ru–Ga thin films.[27] The magnetoresistance (MR), defined as $\mathrm{MR}(\mu_0 H) = (\rho_{xx}(\mu_0 H) - \rho_{xx}(\mu_0 H = 0))/\rho_{xx}(\mu_0 H = 0)$ where ρ_{xx} is the longitudinal resistivity, for $Mn_2Ru_{0.75}V_{0.1}Ga$ and $Mn_{2.05}Ru_{0.75}V_{0.2}Ga$ at different temperatures is shown in Figs. 6(c) and 6(d). At 5 K, the MR of $Mn_2Ru_{0.75}V_{0.1}Ga$ is negative within a magnetic field of 5 T while the MR of $Mn_{2.05}Ru_{0.75}V_{0.2}Ga$ is only negative at low fields and it becomes positive at higher fields. Near the compensation temperature, the signs of MR for both $Mn_2Ru_{0.75}V_{0.1}Ga$ and $Mn_{2.05}Ru_{0.75}V_{0.2}Ga$ reverses. Figures 6(e) and 6(f) show the absolute value of the anomalous Hall conductivity $|\sigma_{\mathrm{AH}}| = |\rho_{yx}|/(\rho_{xx}^2 + \rho_{yx}^2)$ and anomalous Hall angle $|\theta_{\mathrm{AH}}| = |\rho_{yx}|/\rho_{xx}$, against temperature for the two sample. On the whole, $|\sigma_{\mathrm{AH}}|$ and $|\theta_{\mathrm{AH}}|$ are rather smooth across T_{M}, which is expected for an ideal compensated ferrimagnet where the sign reversal of σ_{AH} across T_{M} is solely due to the change of the dominant magnetic sublattice below and above T_{M}, without involving structural or phase transformation. Although we still observe a slight decrease of $|\sigma_{\mathrm{AH}}|$ and $|\theta_{\mathrm{AH}}|$ near T_{M}, most probably caused by minor spatial inhomogeneity of the alloy composition and T_{M}, the inhomogeneity induced complex anomalous Hall effect previously found in epitaxial Mn–Ru–Ga[32] and amorphous Co–Gd[44] compensated ferrimagnetic thin films can be largely mitigated in our annealed bulk samples. Overall, we have shown that the compensated ferrimagnets can show finite anomalous Hall effect even when the net magnetization exactly vanishes at T_{M} and ideally there should be no anomaly in $|\sigma_{\mathrm{AH}}|$ and $|\theta_{\mathrm{AH}}|$ across T_{M}.

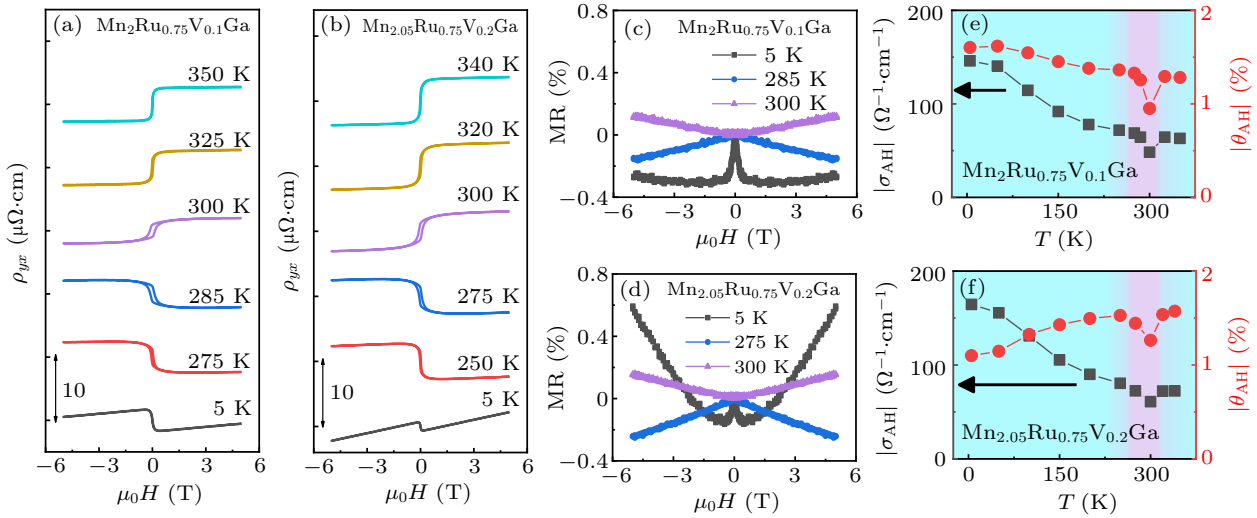


Fig. 6. The Hall effect loops of (a) $Mn_2Ru_{0.75}V_{0.1}Ga$ and (b) $Mn_{2.05}Ru_{0.75}V_{0.2}Ga$ at different temperatures. Magnetoresistance (MR) of (c) $Mn_2Ru_{0.75}V_{0.1}Ga$ and (d) $Mn_{2.05}Ru_{0.75}V_{0.2}Ga$ at different temperatures. Temperature-dependent absolute values of anomalous Hall conductivity $|\sigma_{\mathrm{AH}}|$ (black blocks; left axis) and Hall angle $|\theta_{\mathrm{AH}}|$ (red dots; right axis) of (e) $Mn_2Ru_{0.75}V_{0.1}Ga$ and (f) $Mn_{2.05}Ru_{0.75}V_{0.2}Ga$.

3.5. Scaling of anomalous Hall effect

To separate various contributions to the anomalous Hall effect in a magnetic conductor, a common practice is to study the scaling of σ_{AH} or anomalous Hall resistivity σ_{AH} with the longitudinal conductivity $\sigma_{xx} = \rho_{xx}/(\rho_{xx}^2 + \rho_{yx}^2)$ or longitudinal resistivity ρ_{xx}, which is considered to reflect the transport lifetime, τ.[45] For intrinsic anomalous Hall effect that arises from the Berry curvature of the band structures or the extrinsic anomalous Hall effect due to side jump mechanism, σ_{AH} is independent of σ_{xx} and τ (similarly ρ_{AH} is proportional to ρ_{xx}^2). For extrinsic anomalous Hall effect due to skew scattering, σ_{AH} is proportional to σ_{xx} and τ (or ρ_{AH} is proportional to ρ_{xx}).

The analysis can be further refined by discerning skew scattering contribution due to defects (dominant at low temperature) and thermally-excited quasiparticles, e.g., phonons and magnons (negligible at low temperature).[46] Let $\rho_{xx}(T) = \rho_{xx0} + \rho_{xxT}(T)$, then the general expression of ρ_{AH} will be

$$\rho_{\mathrm{AH}} = a'\rho_{xx0} + a''\rho_{xxT} + b'\rho_{xx0}^2 + b''\rho_{xxT}^2,$$

where a', a'', b', and b'' are fitting parameters, $\rho_{xx0} = \rho_{xx}(T = 4\ \mathrm{K})$ and $\rho_{xxT}(T) = \rho_{xx}(T) - \rho_{xx}(T = 4\ \mathrm{K})$ are the residual resistivity and the resistivity contribution that depends on temperature, respectively.

Obviously, the accuracy of such a separation partly relies on our ability to experimentally tune the range of σ_{xx} and τ, by varying the temperature. Concerning this point, compounds and alloys in bulk form are advantageous compared with those in thin films because they typically possess better atomic ordering and less defect, leading to higher residual resistivity ratio, $\mathrm{RRR} = \rho_{xx}(T = 300\ \mathrm{K})/\rho_{xx}(T = 4\ \mathrm{K})$. In addition, the negligible interfacial scattering in bulk samples allows us to

focus on the electronic transport that is inherent to the bulk properties of the material, and is not related to the interfacial effects that is inevitably involved and dependent on the adjacent layer. This is the reason why our Mn–Ru–V–Ga buttons possess significantly higher RRR than previous Mn–Ru–Ga thin films.[27]

The variation of $|\sigma_{AH}|$ with σ_{xx} for several Mn–Ru–V–Ga alloy samples of varying V content y is shown in Fig. 7(a). Solid and empty symbols represent the data for stoichiometric $Mn_{2.25-y}Ru_{0.75}V_yGa$ and off-stoichiometric $Mn_2Ru_{0.75}V_yGa$ series respectively. On the whole, $|\sigma_{AH}|$ is proportional to σ_{xx} with a nearly constant $|\theta_{AH}| \sim 1\%$, implying that the main contribution of anomalous Hall effect in Mn–Ru–V–Ga is extrinsic skew scattering mechanism. The dependence of anomalous Hall resistivity $|\rho_{AH}|$ with ρ_{xx}^2 are shown in Fig. 7(b). Obviously, $|\rho_{AH}|$ is not linear with ρ_{xx}^2, which again confirms the negligible contribution of the intrinsic mechanism, i.e., b'' is small. Figure 7(c) show the variation of $|\rho_{AH}|$ with ρ_{xxT}. The $|\rho_{AH}|$ shows excellent linear relationship with ρ_{xxT}, indicating that the contribution of thermally-excited phonons, a'', is significant. Note that since the temperature-dependent b'' is negligibly small in the Mn–Ru–V–Ga system, we have also dropped the b' term, which sometimes is attributed to the extrinsic side jump mechanism. Therefore, a relatively simple phenomenological relation $|\rho_{AH}| = a'\rho_{xx0} + a''\rho_{xxT}$ is sufficient to describe all our experimental data. The fact that a' and a'' are of the same sign suggests that the two skew scattering contributions are additive. For comparison, the anomalous Hall effect in epitaxial Fe,[46] Co[47] or $L1_0$–$Mn_{1.5}Ga$ films[48] was found to be governed by the intrinsic mechanism, and the phonon-induced skew scattering can be ignored. Non-negligible phonon skew scattering contribution was also reported in some Heusler alloys,[49–51] although we should note that the conductivity of these systems is in the "moderately dirty regime" with RRR that is close to 1 or even slightly less than 1. Therefore, we believe that it is unclear whether the changes in the anomalous Hall effect with temperature in these systems can be entirely attributed to the phonon-induced skew scattering.

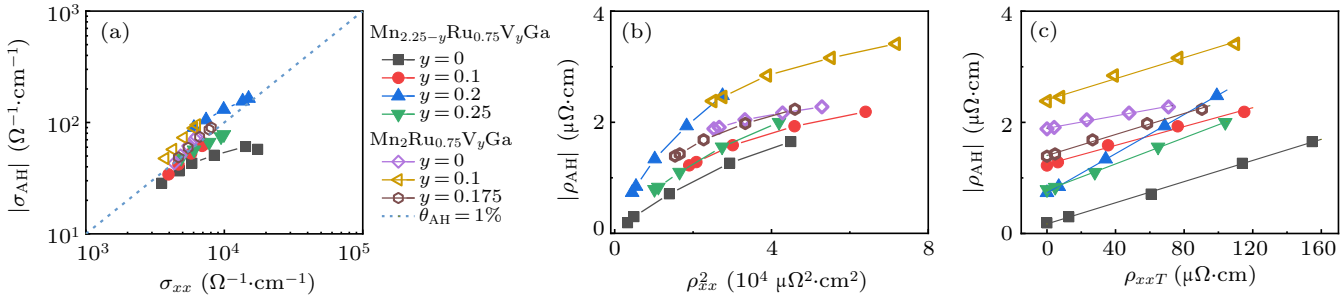


Fig. 7. (a) Anomalous Hall conductivity $|\sigma_{AH}|$ against longitudinal conductivity σ_{xx} in log–log scales. Scaling of the anomalous Hall resistivity $|\rho_{AH}|$ with (b) ρ_{xx}^2 and (c) ρ_{xxT}. Solid symbols and open symbols represent stoichiometric $Mn_{2.25-y}Ru_{0.75}V_yGa$ and off-stoichiometric $Mn_2Ru_{0.75}V_yGa$ series, respectively.

In order to further elucidate how the extrinsic skew scattering evolves with V content y, we plot and compare the RRR of $Mn_2Ru_{0.75}V_yGa$ and $Mn_{2.25-y}Ru_{0.75}V_yGa$ series in Fig. 8(a). Since RRR closely relates to the defects and reflects the overall quality of the sample, it is therefore reasonable to assume that the RRR is correlated with the extrinsic skew scattering to a certain degree. The RRR of $Mn_2Ru_{0.75}V_yGa$ and $Mn_{2.25-y}Ru_{0.75}V_yGa$ are shown in Fig. 8(a). Our first observation is that the stoichiometry of Ga (i.e., maintaining 25 at.% of Ga) has decisive implication on the RRR. For the two ternary alloys $Mn_{2.25}Ru_{0.75}Ga$ (25 at.% of Ga) and $Mn_2Ru_{0.75}Ga$ (26.7 at.% of Ga), RRR of the former is enhanced by more than a factor of 2 than that of the latter. The density measurement suggests that the excess Ga atoms occupy Mn or Ru sites, so we can conclude that these main group element antisites are mainly responsible for the reduction of RRR. A small amount of V first acts as additional scattering center, giving rise to the lowest RRR for $y = 0.1$ of the two series. Then, the RRR increases slightly to ~ 3 upon increasing the V content to $y = 0.25$.

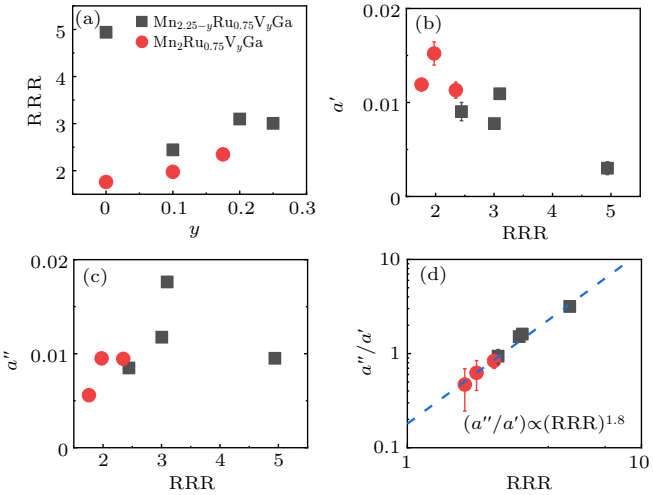


Fig. 8. (a) Variation of residual resistivity ratio (RRR) with V content, y. Variation of (b) a', (c) a'', and (d) a''/a' with RRR.

Figures 8(b)–8(d) show the variation of a', a'', and a''/a' with RRR, respectively. In general, as RRR increases, a' tends to decrease whereas a'' shows the opposite increasing trend. The relative contribution of the two skew scattering mechanisms against the RRR value can be phenomenologically de-

scribed by an intriguing scaling relation $a''/a' \propto \mathrm{RRR}^{1.8}$ spanning over nearly one order of magnitude, as shown in Fig. 8(d). Interestingly, for off-stoichiometric $Mn_2Ru_{0.75}V_yGa$ series (red symbols), the a''/a' ratio is typically less than 1, reflecting the dominant role of extrinsic skew scattering induced by Ga antisite defects, with appreciable y intercept in the $|\rho_{AH}|$ versus ρ_{xxT} plot in Fig. 7(d). In contrast, when 25-at.% Ga stoichiometry is maintained, e.g., for $Mn_{2.25-y}Ru_{0.75}V_yGa$ series (black symbols), the larger-than-unity a''/a' ratio suggests that the thermally-excited phonons make significant contribution to the observed anomalous Hall effect. The observed scaling relation $a''/a' \propto \mathrm{RRR}^{1.8}$ implies that although a' and a'' skew scattering contributions to the anomalous Hall effect in Mn–Ru–V–Ga quaternary alloys are sensitive to RRR and controllable by the composition as well as the atomic ordering, there may be a tradeoff between the two parameters, resulting in a rather constant anomalous Hall angle of $\sim 1\%$. To further enhance the anomalous Hall effect in compensated ferrimagnet, it would be highly desirable to utilize the collective contribution of the intrinsic and extrinsic anomalous Hall effects. Moreover, it would be interesting to test the validity and the universality of such a relation in other magnetic systems. One potential candidate is Fe_3Sn_2,[52] which is known to show large RRR and large extrinsic anomalous Hall effect at low temperature. However, there is an additional complication that the intrinsic contribution, the skew scattering contribution due to defects and that due to phonon should be carefully separated.

4. Conclusions

In summary, we have systematically studied the compensated ferrimagnetic state and anomalous Hall effect scaling in ternary Mn–Ru–Ga and quaternary Mn–Ru–V–Ga-based polycrystalline Heusler compounds prepared by arc melting. Alloying with V stabilizes the cubic Heusler structure and substantially widens the tuning range of the magnetic compensation in these compounds. Detailed analyses of the anomalous Hall effect scaling reveal the dominant role of skew scattering mechanism, for which the contributions of Ga antisite defects and thermally-excited phonons are additive and controllable by varying the composition. These results provide a guideline to design compensated ferrimagnetic state with large anomalous Hall effect in Heusler compounds.

Acknowledgements

Part of this work was carried out at the Synergetic Extreme Condition User Facility (SECUF) and the Center for Materials Genome. We thank H. Z. Zhao and N. Chen for their assistance in the density measurement.

Project supported by the National Key Research and Development Program of China (Grant No. 2022YFA1402600), the National Natural Science Foundation of China (Grant No. 12274438), and the Beijing Natural Science Foundation, China (Grant No. Z230006).

References

[1] Kim S K, Beach G S D, Lee K J, Ono T, Rasing T and Yang H 2022 *Nat. Mater.* **21** 24
[2] Avci C O 2021 *J. Phys. Soc. Jpn.* **90** 081007
[3] Liu Q, Zhu L, Zhang X S, Muller D A and Ralph D C 2022 *Appl. Phys. Rev.* **9** 021402
[4] Zhang H, Koo J, Xu C, Sretenovic M, Yan B and Ke X 2022 *Nat. Commun.* **13** 1091
[5] Graves C E, Reid A H, Wang T, *et al*. 2013 *Nat. Mater.* **12** 293
[6] Woo S, Song K M, Zhang X, Zhou Y, Ezawa M, Liu X, Finizio S, Raabe J, Lee N J, Kim S I, Park S Y, Kim Y, Kim J Y, Lee D, Lee O, Choi J W, Min B C, Koo H C and Chang J 2018 *Nat. Commun.* **9** 959
[7] Radu I, Vahaplar K, Stamm C, Kachel T, Pontius N, Dürr H A, Ostler T A, Barker J, Evans R F L, Chantrell R W, Tsukamoto A, Itoh A, Kirilyuk A, Rasing T and Kimel A V 2011 *Nature* **472** 205
[8] Nayak A K, Nicklas M, Chadov S, Khuntia P, Shekhar C, Kalache A, Baenitz M, Skourski Y, Guduru V K, Puri A, Zeitler U, Coey J M D and Felser C 2015 *Nat. Mater.* **14** 679
[9] Siddiqui S A, Han J, Finley J T, Ross C A and Liu L 2018 *Phys. Rev. Lett.* **121** 057701
[10] Kim K J, Kim S K, Hirata Y, Oh S H, Tono T, Kim D H, Okuno T, Ham W S, Kim S, Go G, Tserkovnyak Y, Tsukamoto A, Moriyama T, Lee K J and Ono T 2017 *Nat. Mater.* **16** 1187
[11] Zhou H A, Xu T, Bai H and Jiang W 2021 *J. Phys. Soc. Jpn.* **90** 081006
[12] Finley J and Liu L 2020 *Appl. Phys. Lett.* **116** 110501
[13] Hirata Y, Kim D H, Kim S, Lee D K, Oh S H, Kim D Y, Nishimura T, Okuno T, Futakawa Y, Yoshikawa H, Tsukamoto A, Tserkovnyak Y, Shiota Y, Moriyama T, Choe S B, Lee K J and Ono T 2019 *Nat. Nanotechnol.* **14** 232
[14] Ghosh S, Komori T, Hallal A, Garcia J P, Gushi T, Hirose T, Mitarai H, Okuno H, Vogel J, Chshiev M, Attané J P, Vila L, Suemasu T and Pizzini S 2021 *Nano Lett.* **21** 2580
[15] Caretta L, Mann M, Büttner F, Ueda K, Pfau B, Günther C M, Hessing P, Churikova A, Klose C, Schneider M, Engel D, Marcus C, Bono D, Bagschik K, Eisebitt S and Beach G S D 2018 *Nat. Nanotechnol.* **13** 1154
[16] Stanciu C D, Tsukamoto A, Kimel A V, Hansteen F, Kirilyuk A, Itoh A and Rasing T 2007 *Phys. Rev. Lett.* **99** 217204
[17] Uemura M, Yamagishi T, Ebisu S, Chikazawa S and Nagata S 2008 *Philos. Mag.* **88** 209
[18] Avci C O, Quindeau A, Pai C F, Mann M, Caretta L, Tang A S, Onbasli M C, Ross C A and Beach G S D 2017 *Nat. Mater.* **16** 309
[19] Rosenberg E R, Beran L, Avci C O, Zeledon C, Song B, Gonzalez-Fuentes C, Mendil J, Gambardella P, Veis M, Garcia C, Beach G S D and Ross C A 2018 *Phys. Rev. Mater.* **2** 094405
[20] Wu H, Xu Y, Deng P, Pan Q, Razavi S A, Wong K, Huang L, Dai B, Shao Q, Yu G, Han X, Rojas-Snchez J C, Mangin S and Wang K L 2019 *Adv. Mater.* **31** 1901681
[21] Streubel R, Lambert C H, Kent N, Ercius P, N'Diaye A T, Ophus C, Salahuddin S and Fischer P 2018 *Adv. Mater.* **30** 1800199
[22] Céspedes-Berrocal D, Damas H, Petit-Watelot S, Maccariello D, Tang P, Arriola-Córdova A, Vallobra P, Xu Y, Bello J L, Martin E, Migot S, Ghanbaja J, Zhang S, Hehn M, Mangin S, Panagopoulos C, Cros V, Fert A and Rojas-Snchez J C 2021 *Adv. Mater.* **33** 2007047
[23] Mitarai H, Komori T, Hirose T, Ito K, Ghosh S, Honda S, Toko K, Vila L, Attané J P, Amemiya K and Suemasu T 2020 *Phys. Rev. Mater.* **4** 094401
[24] Zhang R, He Y, Fruchart D, Coey J M D and Gercsi Z 2022 *Acta Mater.* **234** 118021
[25] Stinshoff R, Nayak A K, Fecher G H, Balke B, Ouardi S, Skourski Y, Nakamura T and Felser C 2017 *Phys. Rev. B* **95** 060410
[26] Banerjee C, Teichert N, Siewierska K E, Gercsi Z, Atcheson G Y P, Stamenov P, Rode K, Coey J M D and Besbas J 2020 *Nat. Commun.* **11** 4444
[27] Kurt H, Rode K, Stamenov P, Venkatesan M, Lau Y C, Fonda E and Coey J M D 2014 *Phys. Rev. Lett.* **112** 027201

[28] Siewierska K E, Atcheson G, Jha A, Esien K, Smith R, Lenne S, Teichert N, O'Brien J, Coey J M D, Stamenov P and Rode K 2021 *Phys. Rev. B* **104** 064414

[29] Betto D, Thiyagarajah N, Lau Y C, Piamonteze, Arrio M A, Stamenov P, Coey J M D and Rode Karsten 2015 *Phys. Rev. B* **91** 094410

[30] Finley J, Lee C H, Huang P Y and Liu L 2019 *Adv. Mater.* **31** 1805361

[31] Jamer M E, Wang Y J, Stephen G M, McDonald I J, Grutter A J, Sterbinsky G E, Arena D A, Borchers J A, Kirby B J, Lewis L H, Barbiellini B, Bansil A and Heiman D 2017 *Phys. Rev. Appl.* **7** 064036

[32] Dou C, Xu X, Yang K, Li C, Zhang T, Zhu Z, Zhao X, Meng K, Wu Y, Chen J, Yang M, Khovalo V V and Jiang Yong 2022 *Appl. Phys. Lett.* **121** 182403

[33] Zhu L, Zhu L, Liu Q and Lin X 2023 *Phys. Rev. B* **108** 014420

[34] Yu J, Liu L, Deng J, Zhou C, Liu H, Poh F and Chen J 2019 *J. Magn. Magn. Mater.* **487** 165316

[35] Davydova M D, Skirdkov P N, Zvezdin K A, Wu J C, Ciou S Z, Chiou Y R, Ye L X, Wu T H, Bhatt R C, Kimel A V and Zvezdin A K 2020 *Phys. Rev. Appl.* **13** 034053

[36] Chen T and Malmhäl R 1983 *J. Magn. Magn. Mater.* **35** 269

[37] Okamoto K and Miura N 1989 *Physica B* **155** 259

[38] Liu G D, Dai X F, Liu H Y, Chen J L, Li Y X, Xiao G and Wu G H 2008 *Phys. Rev. B* **77** 014424

[39] Kübler J 1984 *Physica* **127B** 257

[40] Galanakis I, Dederichs P H and Papanikolaou N 2002 *Phys. Rev. B* **66** 174429

[41] Graf T, Felser C and Parkin S S P 2011 *Prog. Solid State Ch.* **39** 1

[42] Zhang H G, Chen J, Liu E K, Yue M, Liu G D, Lu Q M, Wang W H and Wu G H 2019 *Intermetallics* **106** 71

[43] Kumar K R, Kumar N H, Markandeyulu G, Chelvane J A, Neu V and Babu P D 2008 *J. Magn. Magn. Mater.* **320** 2737

[44] Fu T, Li S, Feng X, Cui Y, Yao J, Wang B, Cao J, Shi Z, Xue D and Fan X 2021 *Phys. Rev. B* **103** 064432

[45] Nagaosa N, Sinova J, Onoda S, MacDonald A H and Ong N P 2010 *Rev. Mod. Phys.* **82** 1539

[46] Tian Y, Ye L and Jin X 2009 *Phys. Rev. Lett.* **103** 087206

[47] Hou D, Li Y, Wei D, Tian D, Wu L and Jin X 2012 *J. Phys.: Condens. Matter* **24** 482001

[48] Zhu L, Pan D and Zhao J H 2014 *Phys. Rev. B* **89** 220406(R)

[49] Xia Z, Zhang Q, Yuan M, Liu Z and Ma X 2023 *J. Alloys Compd.* **937** 168497

[50] Fu H, Li Y, Ma L, You C, Zhang Q and Tian N 2019 *J. Magn. Magn. Mater.* **473** 16

[51] Mishra V, Barwal V, Pandey L, Gupta N K, Hait S, Kumar A, Sharma N, Kumar N and Chaudhary S 2022 *J. Magn. Magn. Mater.* **547** 168837

[52] Ye L, Kang M, Liu J, Cube F, Wicker C R, Suzuki T, Jozwiak C, Bostwick A, Rotenberg E, Bell D C, Fu L, Comin R and Checkelsky J G 2018 *Nature* **555** 638